RESEARCH ARTICLE

Identification of Lung Tumors in Nude Mice Based on the LIBS With Histogram of Orientation Gradients and Support Vector Machine

QIAN-LIN LIAN[1], XIANG-YOU LI[2], BING LU[2], CHEN-WEI ZHU[2], JIANG-TAO LI[2],
AND JIAN-JUN CHEN[1,3]

[1]School of Public Health, Xinjiang Medical University, Ürümqi 830000, China
[2]Wuhan National Laboratory for Optoelectronics (WNLO), Huazhong University of Science and Technology, Wuhan 430074, China
[3]Institute of Medical Engineering and Technology, Xinjiang Medical University, Ürümqi 830000, China

Corresponding author: Jian-Jun Chen (cjjliyan@163.com)

ABSTRACT Early-stage detection of lung tumors helps to reduce patient mortality rates. In this work, we propose a method for diagnosing lung tumors in nude mice through combining laser-induced breakdown spectroscopy (LIBS) with the Histogram of Orientation Gradients (HOG) and Support Vector Machine (SVM). Firstly, the elemental spectral lines and elemental imaging maps for lung tissue are respectively obtained by the LIBS system. Secondly, the HOG is used to obtain the gradient direction relationship of multi-dimensional spectral intensity from LIBS images. The optimal spectral features based on HOG for different biological tissue can be extracted. And then, the SVM model is adopted to determine lung tumors. The results show that, compared to classification models based on SVM with full-spectrum emission intensity and SVM with Principal Component Analysis (PCA), the identification accuracy of lung tumors from the nude mice by using the HOG-SVM can be improved by 10.66% and 4.66%, the sensitivity can be improved by 12% and 4%, and the specificity can be improved by 8% and 6%, respectively. In addition, HOG-SVM is also used to differentiate inflammatory lung tissue from normal lung tissue in nude mice, and achieves the ideal classification result. This work shows that the LIBS technique combined with HOG-SVM provides a complementary method for the rapid detection of lung tumors, contributing to the successful treatment of patients.

INDEX TERMS Laser induced breakdown spectroscopy (LIBS), lung tumor, histogram of orientation gradients (HOG), support vector machine (SVM).

I. INTRODUCTION

Cancer is the second leading cause of death worldwide. According to the World Health Organization, in 2020 there were 2.21 million new cases of lung cancer, while deaths topped the list at 1.8 million [1]. From the latest data from

The associate editor coordinating the review of this manuscript and approving it for publication was Joewono Widjaja.

the National Cancer Center, 3 million people in China died of cancer in 2020. The number of lung cancer deaths was 710,000, accounting for 23.8% of the total cancer deaths [2]. Early symptoms of lung cancer are not obvious and usually would not attract the attention of patients. When the cancer cells spread and metastasize, indicating that the lung cancer has developed to an advanced stage, the cure rate of patients at this time will be very low. Early diagnosis of lung cancer

is crucial in improving cure rates as well as patient survival and quality of life.

To date, several screening methods have been applied in clinical practice for the assistance in lung cancer diagnosis. The internal condition of the lungs can be effectively visualized by chest X-rays and electron computed tomography (CT) scans of the lungs. However, early-stage lung cancer may not be easily recognized on imaging, especially in smaller diameter masses [3]. The most advanced method for detecting lung tumors is positron emission tomography/X-ray computed tomography (PET-CT), which can detect subtle lesions without any clinical symptoms, and achieve early detection of foci and diagnosis of the disease [4]. In addition, the utilization of laboratory tests such as tumor markers is also considered to support the diagnosis of lung tumors. Randell et al. indicated that cytokeratin fragments could help in the identification and diagnosis of lung tumors [5]. Roth et al. applied the circulating DNA, microRNA and cysteine asparaginase activity in blood for lung cancer detection and risk assessment [6]. However, most tumor markers are not specific to malignant tumors, and non-tumorigenic lesions or side effects of treatments could also give false-positive results. In clinic, the ''gold standard'' for diagnosis of lung tumors is the pathologic evaluation of tissue samples [7]. The tissue samples taken from lung lesions by means of the fiber-optic bronchoscopy can be conducted the pathological examinations to obtain qualitative diagnosis of the affected tissue. This method is limited by the subjectivity of pathologists' diagnosis, and cannot provide results timely, affecting the timeliness of treatment decisions. Therefore, there is an urgent need to find experimental techniques for the rapid detection of lung tumor.

Laser induced breakdown spectroscopy (LIBS) is an atomic emission spectroscopy technique based on qualitative and quantitative chemical multi-element analysis [8], [9], [10], [11]. This method allows for fast and simultaneous multi-element analysis with remote, on-line and portable capabilities [12]. Up to now, LIBS has been widely used in geological exploration [13], industrial metallurgy [14], [15], environmental monitoring [16], [17], food safety [18], [19] and other fields [20]. Especially, LIBS has been gradually applied to the biomedical field in recent years. For example, chemical analysis by the aid of LIBS for differentiating hard tissue such as bones and teeth of the human body as well as calcified samples [21], and for the identification of selected bacterial pathogens [22]. In terms of tumor detection, El-Hussen et al. used the LIBS technique to differentiate between tumor tissue and normal tissue in breast and colon cancer, which demonstrated that the degree of tumor metastasis was related to the degree of calcium and magnesium enrichment [23]. Researchers have used LIBS technology in combined with chemometrics methods for the diagnosis and treatment of tumors. Gaudiuso et al. utilized the LIBS technique for early diagnosis of mice with melanoma, where direct analysis of LIBS spectra did not

provide any conclusive results. But by combining machine learning algorithms (SVM, Fisher Discriminant Analysis, and Gradient Boosting), they achieved the differentiation for the normal and diseased mice with 96% accuracy [24]. In addition, Lin et al. applied the LIBS technique combined with the Random Forest Boosting Tree model for distinguishing lung tumors from border tissue, with 98.9% classification accuracy acquired [25].

It is well known that there are differences in the kinds and concentrations of chemical elements in biological tissue, and such differences can provide the theoretical basis for LIBS to differentiate between tissue types. Generally, the most biological tissue only shows moderate trace element variations, there is less variation between classes and concentrations of characteristic spectral lines. Only relying on the intensity characteristics of the spectral lines for differentiation usually did not give satisfactory results. Therefore, digging into the new features of the spectrum is crucial for the application of LIBS technology for tumor identification and diagnosis. The HOG feature is a feature descriptor used in computer vision and image processing, and the technique calculated the number of times the gradient direction occurs locally in an image [26]. This technique has been widely applied in the fields of computer vision [27], [28] and machine learning [29], [30]. The Support Vector Machines (SVM) classifier is a margin-based supervised machine learning method [31] and has been widely used for classification tasks [32], [33]. Dalal and Triggs proposed the HOG feature extraction algorithm in 2005 and combined it with SVM (HOG-SVM) for static pedestrian detection [34]. By means of SVMs and fully-connected neural networks, Goharrizi et al. used HOG features to classify cardiac multi-lead electrocardiogram (ECG) heartbeat with more than 99% classification accuracy [35]. Additionally, based on the algorithms of Real Adaboost and Random Forest, Iwahori et al. utilized HOG features and Hessian filters to promote the performance of automatic detection of polyp detection with higher accuracy, realizing high-precision polyp identification [36]. The studies above mentioned show that HOG features combined with machine learning methods can effectively discriminate similar biological tissue or biological signals. Furthermore, we have noticed that, little work associated with HOG and SVM methods has been applied to identify biological tumor tissue in which the LIBS technique is employed for the multi-element spectra. Unlike pathological staining in the traditional medicine, the LIBS technique can quickly and objectively distinguish the element differences between the malignant tumor tissue and the normal tissue. When spectra of the biological tissue are transmitted into a 2D image, HOG features can simultaneous contain both gradient magnitude and angle relationships between pixels of the image. Hence, HOG features co-established by these two constraint relations are richer and more stable than spectral features consisting of only single-point spectral intensity. For distinguishing malignant tumor from the normal tissue,

the LIBS technique combining HOG and SVM will have a promising way to achieve the improvement of tumor identification from the normal tissue.

In this work, a method based on LIBS technology to achieve lung tumor diagnosis in nude mice is proposed, and the method of HOG feature extraction combined with SVM (HOG-SVM) is applied to the identification of lung tumors. Lung tumor, paraneoplastic tissue and muscle tissue are differentiated in nude mice to validate the proposed method. To further demonstrate the application of the proposed HOG-SVM method in the field of biological tissue identification, classification experiments are also performed on lung tissue in the presence of inflammation and normal lung tissue in nude mice.

II. MATERIALS AND METHODS

A. EXPERIMENTAL SETUP

In this study, tissue samples of lung cancer from the nude mice with the subcutaneous tumor formation are detected using the LIBS technique. The principle is shown in Fig.1. The laser light emitted from the Nd: YAG, Quantel, Big sky, Ultra 100 laser (wavelength 1064 nm, frequency 10 Hz, pulse width 6 ns, and maximum pulse energy 100 mJ) is focused on the sample surface by the reflector and convex lens (focal length 100 mm), and the sample is rapidly ablated to form a plasma. The optical signals generated by the plasma spontaneous radiation are received by a light collector (Ocean Optics, 84-UV-25, detection range 200-2000 nm), and then transmitted through an optical fiber to a middle-order grating spectrometer (Andor Tech., Mechelle 5000) for spectroscopy detection which be connected to an intensified charge-coupled detector (ICCD, Andor Tech., iStar DH-334T). The ICCD converts the optical signals into electrical signals and transmits them to a computer for generating spectrograms.
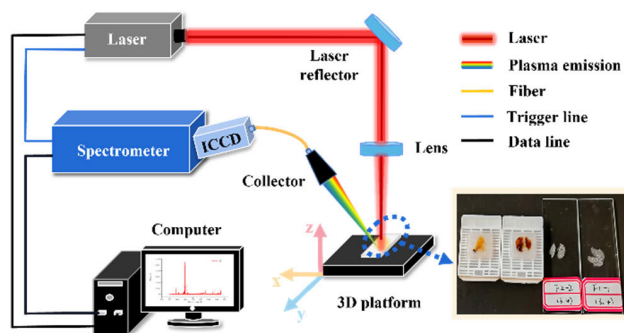

FIGURE 1. Schematic diagram of the LIBS experimental setup.

Three types of tissue including lung tumor, paraneoplastic tissue and muscle tissue are obtained from the nude mice. 50 sections are prepared for each type of tissue, and the corresponding spectra are collected at ten different locations in each section, and the corresponding ten spectra are averaged into one spectrum. And then, the fifty spectra can be obtained for each type of tissue, and the final total spectral number is 150 for all tissue. In addition, elemental mapping experiments will be carried out using the LIBS technique, and the device used in this setup is the commercial laser probe composition analyzer JGTZ-001 developed by Huazhong University of Science and Technology. The device has a built-in laser with a wavelength of 532 nm, which focuses on the surface of the sample with a relatively small spot. Purging argon is used to enhance the signal in the experiment and meanwhile to prevent surface contamination caused by the deposition of flying debris from laser ablation. In order to get an optimized signal-to-noise ratio (SNR), the experimental parameters are subtly adjusted, and the experimental parameters used in this study are kept same during the experiment, with the laser energy of 40 mJ, the acquisition delay of the ICCD detector of 0.7 μs, and the integration time of 10 μs.

B. SAMPLE PRE-PROCESSING

The nude mice are entrusted to Wuhan Huayan Biotechnology Co., Ltd., which can provide nude mice subcutaneous tumor transplantation service, using five Specific Pathogen Free (SPF) grade nude mice (male, 18-22 g). During the experiment, three of these mice are used as the model group (human non-small cell lung cancer cells [A-549] are injected subcutaneously in the right lower abdomen with the number of injected cells) and the remaining two mice are as the control group (cultured at the same time, without any treatment). The samples used here are the tumor tissue, paraneoplastic tissue and nearby muscle tissue from the nude mice in the tumor group. The obtained tissue blocks are paraffin-embedded and the embedded tissue is cut into 5-μm-thin sections. To avoid paraffin contamination of the samples interfering with laser ablation, the samples are subjected to hydration dewaxing and section drying.

Both biological tissue and common slides contain vulgaris chemical elements such as potassium (K), calcium (Ca), sodium (Na), and magnesium (Mg). Ultrathin tissue sections during laser ablation unavoidably suffer from the interference of slide elements. Therefore, quartz slides with 99.999% silica content are applied as substrates in this experiment to prevent interfering elements from affecting the accuracy of the experimental results. In addition, a portion of the obtained lung tumor tissue is used to perform LIBS elemental mapping, one of the sections will be stained for histological hematoxylin and eosin (H&E) staining, and the remaining four adjacent slices are mainly used for imaging of the elements K, Ca, Na, and Mg.

C. DATA ANALYSIS

1) HOG CHARACTERISTICS

The feature extraction is an important part of data processing of biological tissue spectra. By extracting important information from the data, and the good performance for specific biological tissue may be applied in classification and recognition. It is well known that the HOG feature is quite

good at representing localized shapes in terms of intensity gradient and orientation distributions, which can be achieved by separating the whole image into small homogeneous units [37]. The statistical properties possessed by HOG features make the method highly descriptive and robust [38]. The steps for extracting HOG features in this work are as follows:

a: CONVERT SPECTRA TO FEATURE IMAGES

The spectra collected by the spectrometer are the intensity values of the elements in different wavelength ranges and correspond to one-dimensional matrices. HOG features are employed to deal with true color images or 2D grayscale images. Therefore, the one-dimensional spectrum must first be converted to a two-dimensional matrix of M × N. The spectrometer has an effective acquisition range of 200.334 nm-856.513 nm with 23,552 effective pixels for per spectrum. These pixels can be sequentially written into the data structure of the image and saved as a 16-bit gray scale image in Portable Network Graphics (PNG) format [39]. Some pixels might be lost when converting pixels to images. However, these missing pixels have no effect on the results since there are almost no visible peaks at the end of the spectrum. After parameter optimization, the columns and rows of the image are set to 310 and 75, respectively.

b: CALCULATE THE GRADIENT OF THE IMAGE

The process of calculation for the image gradient is illustrated in Fig. 2. Firstly, the spectrum is transformed into a 2D image matrix as shown in the process (1) of Fig. 2. The generated image matrix is divided into blocks, which contains several cells of the same size but not overlaps each other. As shown in the process (1) and (2) of Fig. 2, x and y are the row and column coordinates in the matrix, respectively. $I(x, y)$ is the intensity at the position (x, y) in the matrix. By analogy, the intensities of the pixels at a1, a3, a5 and a7 can be obtained from the corresponding information of the optical spectra. Then the gradient of each pixel of the cell in the horizontal and vertical directions can be calculated according to the Pythagorean theory as shown in process (3). Note that the gradient in the y-direction will be set to 0 if the pixel is located at the top or bottom of the cell, and the gradient in the x-direction will be set to 0 if the pixel is located at the left or right border of the cell [40].

During the gradient calculation for the certain positional coordinates in an image matrix, the horizontal and vertical gradients need to be calculated firstly to get the gradient histogram. The calculation formulas for the gradient $G_x(x, y)$ in the horizontal direction and $G_y(x, y)$ in the vertical direction of the pixel $I(x, y)$ are represented as Eqs. (1) and (2). Then the joint gradient including the magnitude and direction information can be obtained. Accordingly, the calculation formulas for the gradient magnitude $G(x, y)$ and direction θ of the pixel are respectively represented as Eqs. (3) and (4),

$$G_x(x, y) = I(x + 1, y) - I(x - 1, y), \quad (1)$$
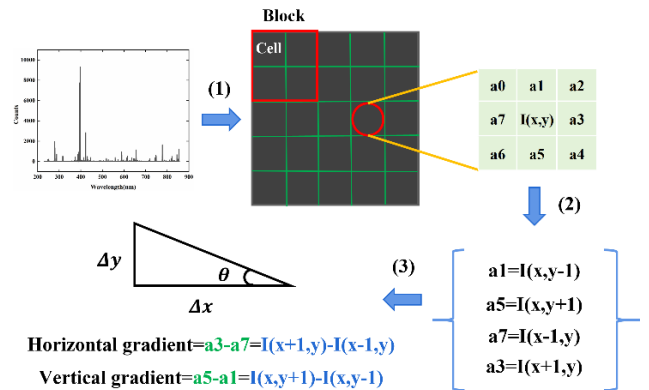

FIGURE 2. Calculate the gradient of the local image.

$$G_y(x, y) = I(x, y + 1) - I(x, y - 1), \quad (2)$$

$$G(x, y) = \sqrt{(G_x(x, y)^2 + G_y(x, y)^2}, \quad (3)$$

$$\theta = \arctan\left[\frac{G_y(x, y)}{G_x(x, y)}\right], \quad (4)$$

where $I(x, y)$ is the intensity at the position of (x, y) in the matrix. x and y are the row and column coordinates in the matrix, respectively [40].

According to the optimization results, the parameters BlockSize (number of cells contained in each block), CellSize (number of pixels contained in each cell), and BolckOverlap (number of overlapping cells between neighboring blocks) used are set to 2, 42, and 1, respectively.

c: CONSTRUCT HISTOGRAM OF THE GRADIENT DIRECTION OF THE CELLS

At first, 180° is evenly divided into several parts, and then, the pixels in each cell are assigned to a fixed angular range according to its gradient direction angle. Next, the gradient values corresponding to the pixels in each angular range are accumulated, and ultimately a histogram of the gradient direction for that cell can be obtained. The average of the histogram of each pixel is calculated to get the gradient vector, and then the cells in the same block are normalized according to this gradient vector. The Numbins (number of directional histogram bins) parameter is set to 9.

d: OBTAIN HOG CHARACTERISTICS

The HOG feature descriptors of a block are obtained by concatenating the gradient histograms of all cells within the block. Accordingly, the HOG features of an image are acquired by concatenating the HOG feature descriptors of all blocks within the image.

2) MODELING AND ASSESSMENT INDICATORS

To build tumor discriminative models, several machine learning methods such as Kernel Extreme Learning Machine (KELM), Random Forest (RF), Fisher Discriminant Analysis (FDA), and SVM have been proposed and implemented.

Due to advantages of fast calculation and robustness to the noise, the SVM model has better classification performance and hence has been widely used in various fields as one of the most effective and popular classification tools [41]. Essentially, SVM is to find an optimal hyperplane that separates the two parts of the linearly divisible n-dimensional data, maximizing the interval between the sample set and the classification hyperplane [42]. Based on the ''one-to-all'', tumor tissue and paraneoplastic tissue are considered as one category for subsequent calculations [43]. A radial basis function is used as the kernel function of the SVM model.
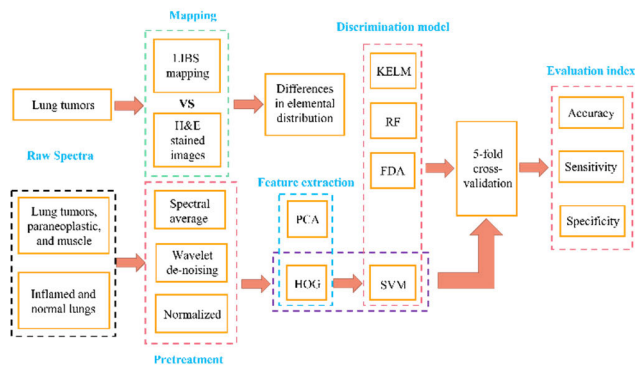

FIGURE 3. Flowchart of model building.

The overall flowchart of model building is shown in Fig. 3. Firstly, LIBS elemental distribution on lung tumor tissue will be mapped and compared with the H&E staining case, which will present the relationship between the differences in elemental distribution and pathological areas. Secondly, after the original spectra are preprocessed, KELM, RF, FDA and SVM models will be built separately, from which the optimal model is selected. To further improve the efficiency of the algorithm, the traditional method PCA is chosen for feature extraction of the LIBS optical spectra from the biological samples. It is considered that the PCA model may suffer from inefficiency in extracting principal components due to the possibility of omitting important information about biological sample differences. As previously mentioned, the HOG method can segment a LIBS image into small connected regions (cells), each of which produces a histogram of directional gradients, and further features the image in terms of a combination of histograms. At the same time, the background and noise in the spectra can be removed and important information is highlighted by means of HOG feature extraction and multivariate analysis. So, the HOG features have a great possibility to better distinguish small differences in the spectra among biological tissue. The HOG feature extraction is chosen to process the spectra and combined with SVM for lung tumor tissue discrimination. In addition, the applicability of the HOG-SVM algorithm will be verified by the identification of inflamed lung tissue and normal lung tissue at the end of this work. To evaluate the stability of the model, a 5-fold cross-validation is utilized in the model. Evaluation indexes of the classification model

including the accuracy, sensitivity, and specificity are taken into account. Here, the accuracy is the ability to determine if a disease tissue of a patient is precisely identified. The sensitivity is the ability of the test to identify the presence of a disease or illness correctly [44]. The higher the sensitivity is, the fewer the false-negative results will be. So, the sensitivity evaluation can contribute to the early detection and treatment of diseases. The specificity is the ability of the test to identify the absence of a disease or illness correctly [44]. The higher the specificity is, the lower the rate of misdiagnosis for patients will be. Through calculating and evaluating the sensitivity and specificity, tumor tissue and paraneoplastic tissue are correspondingly classified as tumor samples, and muscle tissue is as normal tissue samples. In this study, the accuracy, sensitivity, and specificity are calculated according to Eqs. (5), (6), and (7) as follow, respectively,

$$Accuracy = \frac{TP + TN}{TP + FP + TN + FN} \tag{5}$$

$$Sensitivity = \frac{TP}{TP + FN} \tag{6}$$

$$Specificity = \frac{TN}{TN + FP}, \tag{7}$$

where *TP*, *FP*, *TN* and *FN* represent the true positive, false positive, true negative and false negative, respectively [45].

III. RESULTS AND DISCUSSION
A. SPECTRAL ANALYSIS
The average spectra of lung tumor, paraneoplastic tissue, and muscle tissue are shown in Fig. 4. The elemental spectral lines labeled in the spectra are based on the National Institute of Standards and Technology database. Strong element spectral lines for carbon (C), nitrogen (N), hydrogen (H), oxygen (O), CN-band, Ca, Na, and Mg are clearly observed in all three types of tissue in Fig. 4. The spectral line intensity of the element K is very weak and almost cannot be observed in the spectrum due to the low content of the element and little ablation of the sample.
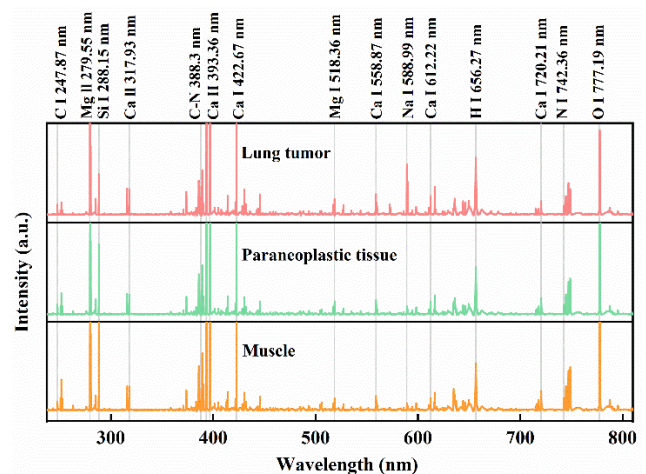

FIGURE 4. Average LIBS spectra of the lung tumor tissue, paraneoplastic tissue and muscle tissue after wavelet noise elimination.

Accordingly, Figure 5 shows the local spectral differences of the lung tumor, paraneoplastic tissue, and muscle tissue. From this diagram, the spectral intensity of Na in lung tumor tissue is obviously higher than that in paraneoplastic tissue and muscle tissue, while Ca and Mg elements also exhibit differences in the three types of tissue. It should be pointed out that, during the experiment, the atomic emission lines of the H, N, and O are not included in the analysis due to the experiments environment performed in the atmosphere. It can be seen in Fig. 4 and Fig. 5 that the tested biological tissue displays small differences of the element spectral line, which isn't beneficial to the discriminative and diagnosis between the focal tissue and normal tissue.
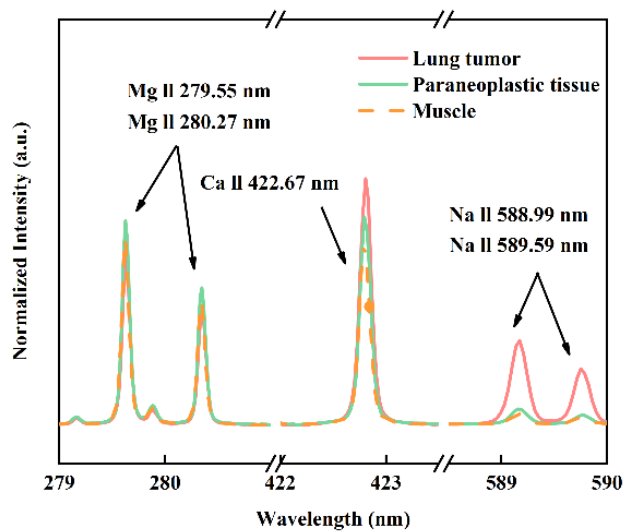

FIGURE 5. Local spectral difference of the lung tumor tissue, paraneoplastic tissue and muscle tissue.

B. ELEMENTAL MAPPING

Mapping the elements distribution of interest may reveal differences in the content and spatial distribution of chemical elements in tumors, which can pave the foundation for the next step in tumor diagnosis [46]. By ablating samples of lung tumor tissue sections using the JGTZ-001 analyzer developed at Huazhong University of Science and Technology, LIBS spectra can be obtained for the lung tumor tissue in which the interest element is correspondingly located. The scanning area of each sample is 7.6 mm × 7.6 mm, which provides a sufficient range to contain the entire sample. The scanning step is set to 100 μm and 5776 spectra are collected for each sample. The spectral line intensities of Na, Mg, K, and Ca for the scanned samples are extracted, respectively, and the one-dimensional spectral line intensities can be converted to two-dimensional matrices. By aid of pseudo-coloring, a contour plot associated with the two-dimensional matrix for the special element distribution can be visualized. During all experiments, the scanning power generated from the laser in the LIBS system is set to the same level, and the scanning acquisition delay and integration time of the

experiment system are kept uniform, so that the acquired elemental distribution maps for different element styles are strictly comparable.

Comparing the pathologically stained images of the tissue with the images of the LIBS feature elements can provide the information of the element distribution. Figure 6 shows the scanned images of LIBS elements of lung tumor tissue from subcutaneously transplanted nude mice. As shown in these diagrams, The H&E-stained image of lung tumor tissue is displayed in Fig. 6(a), and the LIBS images of Na, Mg, K and Ca elements are shown in Figs. 6(b), 6(c), 6(d) and 6(e), respectively. In Fig. 6(a), some identified areas corresponding to the tumor tissue, normal tissue and muscle tissue are respectively marked by capital letter T, N, and M from the pathologist. As can be seen in Figs. 6(b)-6(e), the concentrations of the elements Na, Mg and Ca in the tumor tissue are higher than those in the normal tissue and muscle tissue, while the concentration of the element K in the tumor tissue is slightly lower than that in normal tissue as a whole. In the internal region of the tumor tissue, the elemental distributions for Na, Mg, and Ca also behave heterogeneous in view of LIBS imaging maps. Note that, the concentration of Na element in Fig. 6(b) is obviously stronger in the lower right area of the T region than that on the left side of T region, while the Mg and Ca elements shown in Fig. 6(c) and Fig. 6(e) are mainly aggregated in the bottom half of the tumor, and demonstrate similar concentration variations within tumor tissue, normal tissue, and muscle tissue. It can be seen that the special element distribution can characterize the biological tissue which may be considered as a way to identify the tumor tissue. Furthermore, the pathological staining for the lung tumor tissue do not reveal such differences described above. These results show the tumor and the surrounding non-tumor tissue can exhibit the different element distributions and concentrations in the LIBS imaging maps. Compared to the conventional histopathology, the highly complementary nature of LIBS elemental imaging can contribute to a new means for the auxiliary medical diagnosis.
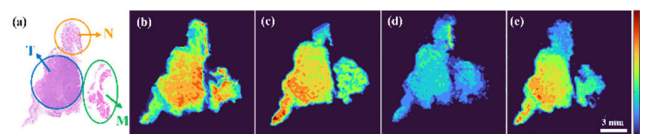

FIGURE 6. Elemental imaging maps of LIBS of lung tumor tissue in nude mice. (a) H&E staining map; (b) Na I 588.99 nm; (c) Mg I 285.21 nm; (d) K I 766.49 nm; (e) Ca I 422.67 nm.

C. DIAGNOSIS OF LUNG TUMOR TISSUE

1) SVM FOR TUMOR DIAGNOSIS

In order to further explore the better tactics for the classification and identification of lung tumor, next the SVM model is applied to differential diagnosis of lung tumor tissue. As seen in subsection II-B, all of 150 spectra will be collected for the SVM model. The raw spectral data from the 150 spectra is transferred into the SVM classifier and the

corresponding output accounts for the average classification accuracy. In this work, the average classification accuracy (sensitivity or specificity) is defined as the mean value from the corresponding classification results of the lung tumor, paraneoplastic tissue, and muscle tissue. To make a fully use of the data, a 5-fold cross-validation method is employed to train the discriminative model by dividing the data into 5 parts, where one part serves as the test set and the remaining four parts are as training sets. During the calculation, the test set will be replaced by one of the training sets for each calculation. Ultimately, the calculation results for the 5 discriminative models can be obtained, and then the average value is taken as the final result.

Figure 7 shows the classification results of SVM based on the full-spectrum emission intensity from the 150 spectra data belonging to 3 classes of tissue (lung tumor, paraneoplastic tissue, and muscle). As a result, the way of SVM gives the average classification accuracies of 84.67%, sensitivity of 85%, and specificity of 84%. As shown in the diagram, few tumor tissue samples are discriminated as paraneoplastic tissue and muscle tissue, the incorrect number of classified samples between the paraneoplastic tissue and muscle is relatively high, in which some samples of the paraneoplastic tissue are misidentified as the muscle tissue and vice versa. Therefore, the classification accuracy of distinguishing these two types of samples is unfavorable. The reason is that the paraneoplastic tissue and muscle tissue have a high spectral similarity, which is adverse to the accurate classification.
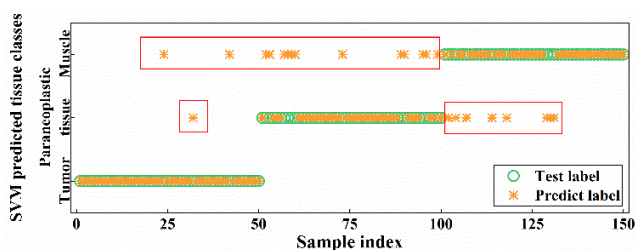

FIGURE 7. Classification results of SVM for the lung tumor, paraneoplastic tissue, and muscle.

2) PCA-SVM FOR TUMOR DIAGNOSIS

LIBS spectral data of lung tissue possesses the high-dimensional and complex characteristics, but not all of the data is the valid signals because there is a great deal of background noise in the spectral data. When the LIBS spectral data is modeled, the noise information will not only aggravate the complexity of the model and cause a "dimensional disaster", but also make the model to be interfered with by the redundant information, which can significantly reduce the classification effectiveness of the lung tissue. Therefore, the extraction of important signals from LIBS spectra is quite important for the recognition of biological tissue. It is well known that the PCA recombines the original variables into a new set of linearly uncorrelated composite variables, which can reduce the influence of the

noise signals. SVM divides the data into two parts based on hyperplane, which is a supervised classification method with good performance. In the previous report, the cervical cancer tissue has been identified using a combined method of PCA and SVM and demonstrated that there exists an obvious spectra difference in trace element content between normal and cancerous tissue. This result shows that PCA associated with LIBS techniques can provide a convenient method for real-time diagnosis of cancer tissues [47]. As a result, the PCA is utilized for feature extraction of the dataset, followed by SVM for identification and diagnosis of lung tumor tissue.

The principal component scores and cumulative contributions of the three types of samples are shown in Fig. 8. From this diagram, the lung tumors are completely distinguished from paraneoplastic and muscle tissue on the projection of principal component 1 (PC1). However, the paraneoplastic and muscle tissue are intertwined and indistinguishable on the projections of principal components 2 (PC2), which well verifies the problem found in the subsection III-C1. The PCA is used to calculate the contribution rate of each eigenvalue, and the 17 eigenvalues with a cumulative contribution rate of 95% are taken as the final eigenvectors. Based on the 5-fold cross-validation results, the average classification accuracy is obtained as 90.67%, and the sensitivity and specificity are 93% and 86%, respectively. Compared with SVM based on the full-spectrum emission intensity, the classification accuracy for the three types of tissue is evidently improved. Note that, the PCA implemented in the classification for feature extraction reduces the complexity of the model and shortens the modeling time. However, the high dimensionality of spectral data requires a large number of computations costs more time when using PCA for principal component extraction. In addition, although the selection of principal components with a cumulative contribution rate of 95% can represent most of the information, some principal components with a smaller contribution rate may also contain important information about the sample differences.

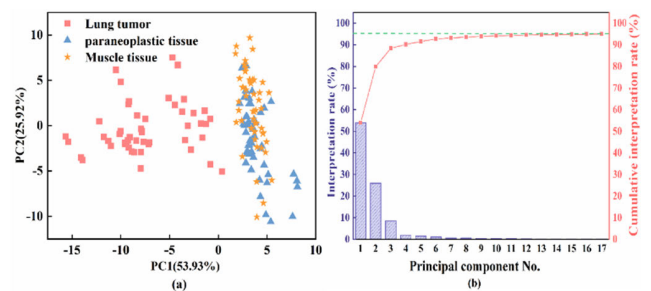**FIGURE 8.** PCA scores of lung tumor tissue, paraneoplastic tissue and muscle tissue samples along PC1, PC2 (a); contribution of each principal component as well as cumulative contribution (b).

3) HOG-SVM FOR TUMOR DIAGNOSIS

Although the PCA-SVM can improve the accuracy of the classification to a certain extent, the related algorithms of the PCA are time-consuming and information-losing.

Due to better advantages of simplicity, fast calculation and robustness to the noise, the HOG algorithm is desirable to be an effective measure quantifier to evaluate quantitatively the classification accuracy of biological tissue. By applying the HOG algorithm in the spectral data of three styles of tissue (tumor, paraneoplastic tissue, and muscle), the small differences in the spectral can be detected by the gradient or edge information from the LIBS image. Figure 9 displays the classification results of SVM based on the HOG algorithm. During the calculation, extraction of features using HOG for all data from 150 LIBS images of lung tumors, paraneoplastic tissue, and muscle tissue according to the method mentioned in the previous subsection II-C1, and then 900 feature variables for the three styles of tissue can be obtained. Next, under the five-fold cross-validation for training of the model, the extracted features of the tissue are as inputs into the SVM to assess the classification accuracy of the different biological tissue. As shown in Fig. 9, the classification accuracies of HOG-SVM reach a high level for the lung tumor, paraneoplastic tissue, and muscle. Among them, all the lung tumor tissue samples are successfully discriminated and classified. The classification accuracies of the paraneoplastic samples and muscle tissue samples are up to 94% and 92%, respectively. The reasons for the improved classification accuracy of HOG-SVM over PCA-SVM can be explained that HOG algorithm can acquire the gradient direction relationship of the normalized multidimensional spectral intensities, which less affects the spectral stability of the tissue. In addition, the multidimensional spectral data derived from the HOG-SVM possesses the more effective information than that for the one-dimensional spectral data from the PCA-SVM.
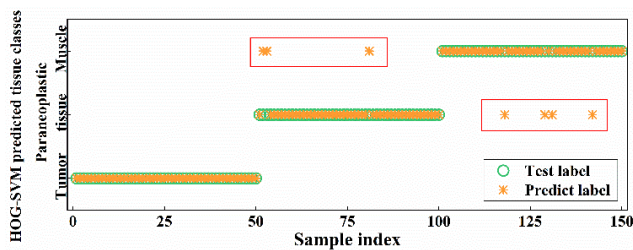

FIGURE 9. Classification results of HOG-SVM for the lung tumor, paraneoplastic tissue, and muscle.

TABLE 1. Average classification accuracy of SVM, PCA-SVM and HOG-SVM models for lung tumor discrimination.

Model	Accuracy (%)	Sensitivity (%)	Specificity (%)
SVM	84.67	85	84
PCA-SVM	90.67	93	86
HOG-SVM	95.33	97	92

Combining with the average classification results of SVM, PCA-SVM, and HOG-SVM presented in Table 1, it can be seen that the average classification accuracy

using HOG-SVM model is 95.33%, sensitivity is 97%, and specificity is 92%. Comparing to the case of SVM, the average classification accuracy, sensitivity, and specificity of HOG-SVM have been improved by 10.66%, 12% and 8% respectively. In contrast with the classification result of PCA-SVM, the HOG-SVM is still able to provide the obviously higher classification accuracy, sensitivity and specificity than the case for the PCA-SVM. The above results indicate that, for the lung tumor, paraneoplastic tissue, and muscle, the HOG-SVM is preferred to obtain the precise identification and classification, which may contribute to the auxiliary diagnosis of lung tumor for clinicians.

4) DIFFERENTIATION OF INFLAMMATORY TISSUE FROM NORMAL LUNG TISSUE
Without loss of generality, the HOG-SVM is further used to distinguish the inflammatory tissue from the normal lung tissue of nude mice through the model group and the normal group. As is diagnosed by the pathologist based on the H&E staining results of the lung tissue sections of the model group, inflammatory infection exists in the lung tissue of the model group of nude mice. Similar to the treatment of the samples as described in 2.1, the inflammatory tissue and normal lung tissue are provided, and the corresponding number of sample sections is 100 for each tissue. By means of the LIBS technique, 100 spectra are acquired for each type of tissue. By comparison, the performance of spectral lines from the lung inflammatory tissue and normal lung tissue show little difference, which may be attributed to the similar element composition of the two types of samples. Next, the spectral data generated from the inflammatory tissue and normal lung tissue is modeled using SVM with full-spectrum emission intensity, PCA-SVM and HOG-SVM, respectively. After the calculation of the five-fold cross-validation, the finally results have been demonstrated in Table 2. As seen in the Table, for the HOG-SVM, the average classification accuracy is 93%, sensitivity is 95% and specificity is 91%, respectively. Compared to the cases of SVM with full-spectrum emission intensity and PCA-SVM, the HOG-SVM can achieve the better classification results in the identification of inflammatory and normal lung tissue. The generalized effectiveness predicts that the HOG-SVM method can be applied to the field of identification of different lung tissue and diagnosis of inflammatory tissue from normal lung tissue.

TABLE 2. Average classification accuracy of SVM, PCA-SVM and HOG-SVM models for inflammatory lung discrimination.

Model	Accuracy (%)	Sensitivity (%)	Specificity (%)
SVM	87.5	88	87
PCA-SVM	91.5	94	89
HOG-SVM	93	95	91

The above results show that, the HOG method combined with SVM based on LIBS spectral information can achieve the identification of lung tumor tissue and inflammatory lung tissue in nude mice, and acquire the relatively ideal classification results. Based on previous research experience on the identification of biological tissue under LIBS technique and classification algorithm, it can be predicted that, the LIBS combined with HOG-SVM proposed in this work has a potential in other types of tumor tissue identification. This work proposes a theoretical and experimental basis for the final application in human clinic, and the study results provide a useful reference for real-time diagnosis of cancer tissue.

IV. CONCLUSION

In summary, we combined the LIBS with the HOG-SVM method to explore the discrimination and diagnosis of lung tumors in nude mice. The results demonstrated that the tested lung tumor, paraneoplastic tissue, and muscle tissue display the small spectral differences of the chemical elements, which is not suitable for the precise discrimination of lung tumors. By converting LIBS spectra to elemental imaging maps, the lung tumor and the surrounding non-tumor tissue presented the different element distributions and concentrations. Furthermore, compared to the cases for the SVM based on full-spectrum emission intensity and SVM-PCA, the HOG-SVM method can obviously improve the average classification accuracy, sensitivity and specificity of the different lung tissue, which can reach 95.33%, 97% and 92%, respectively. Besides, the differential classification of inflammatory lung tissue in nude mice and lung tissue in normal nude mice also verify the generalized effectiveness of HOG-SVM method. After the 5-fold cross-validation, the average classification accuracy can be up to 93%, the sensitivity 95%, and the specificity 91% for the HOG-SVM method. Although the HOG-SVM algorithm based on LIBS spectra in this work achieves the discrimination of lung cancer tissue and inflammation tissue in nude mice, and finally reaches 95.33% and 93% accuracy, it still has the following limitations: (1) The HOG-SVM extracts the gradient features of an image to implement classification, but the process of classification requires a relative more adequate sample capacity. (2) The HOG-SVM model still belongs to a semi-automatic model, which should be downscaled by extracting image features in an artificial way. It is a necessary requirement that the classification executor needs the model design experience of the HOG-SVM. To conclude, this study showed the potential of LIBS techniques combined with the HOG-SVM for clinical diagnosis of lung tumors. Further studies on the discrimination and diagnosis of human lung tumors will be conducted in the future with the aim of revealing the link between lung tumors and chemical elements.

REFERENCES

[1] WHO. (Feb. 2022). *Cancer*. [Online]. Available: https://www.who.int/news-room/fact-sheets/detail/cancer

[2] R. Zheng, S. Zhang, H. Zeng, S. Wang, K. Sun, R. Chen, L. Li, W. Wei, and J. He, "Cancer incidence and mortality in China, 2016," *J. Nat. Cancer Center*, vol. 2, no. 1, pp. 1–9, Mar. 2022.

[3] K. Scherer, A. Yaroshenko, D. A. Bölükbas, L. B. Gromann, K. Hellbach, F. G. Meinel, M. Braunagel, J. V. Berg, O. Eickelberg, M. F. Reiser, F. Pfeiffer, S. Meiners, and J. Herzen, "X-ray dark-field radiography–in-vivo diagnosis of lung cancer in mice," *Sci. Rep.*, vol. 7, no. 1, pp. 1–12, Mar. 2017.

[4] G. K. von Schulthess, H. C. Steinert, and T. F. Hany, "Integrated PET/CT: Current applications and future directions," *Radiology*, vol. 238, no. 2, pp. 405–422, Feb. 2006.

[5] S. H. Randell, H. Dang, and J. L. V. Broers, "The use of keratins as lung cell differentiation markers and as a diagnostic tool in lung cancer" in *Encyclopedia of Respiratory Medicine*, S. M. Janes, Ed., 2nd ed. Oxford, U.K.: Academic, 2022, pp. 694–701.

[6] C. Roth, S. Kasimir-Bauer, K. Pantel, and H. Schwarzenbach, "Screening for circulating nucleic acids and caspase activity in the peripheral blood as potential diagnostic tools in lung cancer," *Mol. Oncol.*, vol. 5, no. 3, pp. 281–291, Jun. 2011.

[7] P. A. VanderLaan, N. Yamaguchi, E. Folch, D. H. Boucher, M. S. Kent, S. P. Gangadharan, A. Majid, M. A. Goldstein, M. S. Huberman, O. N. Kocher, and D. B. Costa, "Success and failure rates of tumor genotyping techniques in routine pathological samples with non-small-cell lung cancer," *Lung Cancer*, vol. 84, no. 1, pp. 39–44, Apr. 2014.

[8] J. Li, M. Xu, Q. Ma, N. Zhao, X. Li, Q. Zhang, L. Guo, and Y. Lu, "Sensitive determination of silicon contents in low-alloy steels using micro laser-induced breakdown spectroscopy assisted with laser-induced fluorescence," *Talanta*, vol. 194, pp. 697–702, Mar. 2019.

[9] B. Campanella, E. Grifoni, S. Legnaioli, G. Lorenzetti, S. Pagnotta, F. Sorrentino, and V. Palleschi, "Classification of wrought aluminum alloys by artificial neural networks evaluation of laser induced breakdown spectroscopy spectra from aluminum scrap samples," *Spectrochimica Acta B, At. Spectrosc.*, vol. 134, pp. 52–57, Aug. 2017.

[10] X. Yang, X. Li, Z. Cui, G. Yao, Z. Zhou, and K. Li, "Improving the sensitivity of surface-enhanced laser-induced breakdown spectroscopy by repeating sample preparation," *Frontiers Phys.*, vol. 8, p. 194, Jun. 2020.

[11] Z. Hao, L. Liu, M. Shen, R. Zhou, J. Li, L. Guo, X. Li, Y. Lu, and X. Zeng, "Long-term repeatability improvement of quantitative LIBS using a two-point standardization method," *J. Anal. At. Spectrometry*, vol. 33, no. 9, pp. 1564–1570, 2018.

[12] L. Brunnbauer, Z. Gajarska, H. Lohninger, and A. Limbeck, "A critical review of recent trends in sample classification using laser-induced breakdown spectroscopy (LIBS)," *TrAC Trends Anal. Chem.*, vol. 159, Feb. 2023, Art. no. 116859.

[13] A. M. Ollila, J. Lasue, H. E. Newsom, R. A. Multari, R. C. Wiens, and S. M. Clegg, "Comparison of two partial least squares-discriminant analysis algorithms for identifying geological samples with the ChemCam laser-induced breakdown spectroscopy instrument," *Appl. Opt.*, vol. 51, no. 7, pp. B130–B142, 2012.

[14] S. Kashiwakura and K. Wagatsuma, "Optimization of partial-least-square regression for determination of manganese in low-alloy steel by single-shot laser-induced breakdown spectroscopy," *ISIJ Int.*, vol. 58, no. 9, pp. 1705–1710, 2018.

[15] Z. Q. Hao, C. M. Li, M. Shen, X. Y. Yang, K. H. Li, L. B. Guo, X. Y. Li, Y. F. Lu, and X. Y. Zeng, "Acidity measurement of iron ore powders using laser-induced breakdown spectroscopy with partial least squares regression," *Opt. Exp.*, vol. 23, no. 6, p. 7795, 2015.

[16] D. Stefas, N. Gyftokostas, E. Bellou, and S. Couris, "Laser-induced breakdown spectroscopy assisted by machine learning for plastics/polymers identification," *Atoms*, vol. 7, no. 3, p. 79, Aug. 2019.

[17] G. A. Lithgow, A. L. Robinson, and S. G. Buckley, "Ambient measurements of metal-containing $PM_{2.5}$ in an urban environment using laser-induced breakdown spectroscopy," *Atmos. Environ.*, vol. 38, no. 20, pp. 3319–3328, Jun. 2004.

[18] E. Bellou, N. Gyftokostas, D. Stefas, O. Gazeli, and S. Couris, "Laser-induced breakdown spectroscopy assisted by machine learning for olive oils classification: The effect of the experimental parameters," *Spectrochimica Acta B, At. Spectrosc.*, vol. 163, Jan. 2020, Art. no. 105746.

[19] M. Yao, H. Yang, L. Huang, T. Chen, G. Rao, and M. Liu, "Detection of heavy metal Cd in polluted fresh leafy vegetables by laser-induced breakdown spectroscopy," *Appl. Opt.*, vol. 56, no. 14, p. 4070, 2017.

[20] Q. Zeng, L. Guo, X. Li, C. He, M. Shen, K. Li, J. Duan, X. Zeng, and Y. Lu, "Laser-induced breakdown spectroscopy using laser pulses delivered by optical fibers for analyzing Mn and Ti elements in pig iron," *J. Anal. At. Spectrometry*, vol. 30, no. 2, pp. 403–409, 2015.

[21] V. K. Singh, V. Kumar, and J. Sharma, "Importance of laser-induced breakdown spectroscopy for hard tissues (bone, teeth) and other calcified tissue materials," *Lasers Med. Sci.*, vol. 30, no. 6, pp. 1763–1778, Aug. 2015.

[22] J. Kaiser, K. Novotný, M. Z. Martin, A. Hrdlička, R. Malina, M. Hartl, V. Adam, and R. Kizek, "Trace elemental analysis by laser-induced breakdown spectroscopy—Biological applications," *Surf. Sci. Rep.*, vol. 67, nos. 11–12, pp. 233–243, Dec. 2012.

[23] A. El-Hussein, A. K. Kassem, H. Ismail, and M. A. Harith, "Exploiting LIBS as a spectrochemical analytical technique in diagnosis of some types of human malignancies," *Talanta*, vol. 82, no. 2, pp. 495–501, Jul. 2010.

[24] R. Gaudiuso, E. Ewusi-Annan, N. Melikechi, X. Sun, B. Liu, L. F. Campesato, and T. Merghoub, "Using LIBS to diagnose melanoma and biomedical fluids deposited on solid substrates: Limits of direct spectral analysis and capability of machine learning," *Spectrochimica Acta B, At. Spectrosc.*, vol. 146, pp. 106–114, Aug. 2018.

[25] X. Lin, H. Sun, X. Gao, Y. Xu, Z. Wang, and Y. Wang, "Discrimination of lung tumor and boundary tissues based on laser-induced breakdown spectroscopy and machine learning," *Spectrochimica Acta B, At. Spectrosc.*, vol. 180, Jun. 2021, Art. no. 106200.

[26] A. K. Sharma, A. Nandal, A. Dhaka, K. Polat, R. Alwadie, F. Alenezi, and A. Alhudhaif, "HOG transformation based feature extraction framework in modified ResNet50 model for brain tumor detection," *Biomed. Signal Process. Control*, vol. 84, Jul. 2023, Art. no. 104737.

[27] S. Ramachandra and S. Ramachandran, "Region specific and subimage based neighbour gradient feature extraction for robust periocular recognition," *J. King Saud Univ.-Comput. Inf. Sci.*, vol. 34, no. 10, pp. 7961–7973, Nov. 2022.

[28] D. Lakshmi and R. Ponnusamy, "Facial emotion recognition using modified HOG and LBP features with deep stacked autoencoders," *Microprocessors Microsyst.*, vol. 82, Apr. 2021, Art. no. 103834.

[29] L. Cai, J. Zhu, H. Zeng, J. Chen, C. Cai, and K.-K. Ma, "HOG-assisted deep feature learning for pedestrian gender recognition," *J. Franklin Inst.*, vol. 355, no. 4, pp. 1991–2008, Mar. 2018.

[30] B. Nassih, A. Amine, M. Ngadi, and N. Hmina, "DCT and HOG feature sets combined with BPNN for efficient face classification," *Proc. Comput. Sci.*, vol. 148, pp. 116–125, Jan. 2019.

[31] R. Kashef, "A boosted SVM classifier trained by incremental learning and decremental unlearning approach," *Expert Syst. Appl.*, vol. 167, Apr. 2021, Art. no. 114154.

[32] D. Keerthana, V. Venugopal, M. K. Nath, and M. Mishra, "Hybrid convolutional neural networks with SVM classifier for classification of skin cancer," *Biomed. Eng. Adv.*, vol. 5, Jun. 2023, Art. no. 100069.

[33] D. He, D. Ren, Z. Guo, and B. Jiang, "Insomnia disorder diagnosed by resting-state fMRI-based SVM classifier," *Sleep Med.*, vol. 95, pp. 126–129, Jul. 2022.

[34] N. Dalal and B. Triggs, "Histograms of oriented gradients for human detection," in *Proc. IEEE Comput. Soc. Conf. Comput. Vis. Pattern Recognit.*, Jun. 2005, pp. 886–893.

[35] M. A. Sheikh Beig Goharrizi, A. Teimourpour, M. Falah, K. Hushmandi, and M. S. Isfeedvajani, "Multi-lead ECG heartbeat classification of heart disease based on HOG local feature descriptor," *Comput. Methods Programs Biomed. Update*, vol. 3, Jan. 2023, Art. no. 100093.

[36] Y. Iwahori, H. Hattori, Y. Adachi, M. K. Bhuyan, R. J. Woodham, and K. Kasugai, "Automatic detection of polyp using Hessian filter and HOG features," *Proc. Comput. Sci.*, vol. 60, pp. 730–739, Jan. 2015.

[37] Z. Sun, E. Caetano, S. Pereira, and C. Moutinho, "Employing histogram of oriented gradient to enhance concrete crack detection performance with classification algorithm and Bayesian optimization," *Eng. Failure Anal.*, vol. 150, Aug. 2023, Art. no. 107351.

[38] H. Zhou and G. Yu, "Research on pedestrian detection technology based on the SVM classifier trained by HOG and LTP features," *Future Gener. Comput. Syst.*, vol. 125, pp. 604–615, Oct. 2021.

[39] J. Yan, P. Yang, Z. Hao, R. Zhou, X. Li, S. Tang, Y. Tang, X. Zeng, and Y. Lu, "Classification accuracy improvement of laser-induced breakdown spectroscopy based on histogram of oriented gradients features of spectral images," *Opt. Exp.*, vol. 26, no. 22, p. 28996, Oct. 2018.

[40] J. Chen, K. Zhan, Q. Li, Z. Tang, C. Zhu, K. Liu, and X. Li, "Spectral clustering based on histogram of oriented gradient (HOG) of coal using laser-induced breakdown spectroscopy," *J. Anal. At. Spectrometry*, vol. 36, no. 6, pp. 1297–1305, 2021.

[41] H. Wang, G. Li, and Z. Wang, "Fast SVM classifier for large-scale classification problems," *Inf. Sci.*, vol. 642, Sep. 2023, Art. no. 119136.

[42] M. Çakir, M. Yilmaz, M. A. Oral, H. Ö. Kazanci, and O. Oral, "Accuracy assessment of RFerns, NB, SVM, and kNN machine learning classifiers in aquaculture," *J. King Saud Univ.-Sci.*, vol. 35, no. 6, Aug. 2023, Art. no. 102754.

[43] G. Wu, C. Li, L. Yin, J. Wang, and X. Zheng, "Compared between support vector machine (SVM) and deep belief network (DBN) for multi-classification of Raman spectroscopy for cervical diseases," *Photodiagnosis Photodyn. Therapy*, vol. 42, Jun. 2023, Art. no. 103340.

[44] A. G. Lalkhen and A. McCluskey, "Clinical tests: Sensitivity and specificity," *Continuing Educ. Anaesthesia Crit. Care Pain*, vol. 8, no. 6, pp. 221–223, Dec. 2008.

[45] B. S. Idrees, Q. Wang, M. N. Khan, G. Teng, X. Cui, W. Xiangli, and K. Wei, "In-vitro study on the identification of gastrointestinal stromal tumor tissues using laser-induced breakdown spectroscopy with chemometric methods," *Biomed. Opt. Exp.*, vol. 13, no. 1, p. 26, Jan. 2022.

[46] S. Moncayo, F. Trichard, B. Busser, M. Sabatier-Vincent, F. Pelascini, N. Pinel, I. Templier, J. Charles, L. Sancey, and V. Motto-Ros, "Multi-elemental imaging of paraffin-embedded human samples by laser-induced breakdown spectroscopy," *Spectrochimica Acta B, At. Spectrosc.*, vol. 133, pp. 40–44, Jul. 2017.

[47] J. Wang, L. Li, P. Yang, Y. Chen, Y. Zhu, M. Tong, Z. Hao, and X. Li, "Identification of cervical cancer using laser-induced breakdown spectroscopy coupled with principal component analysis and support vector machine," *Lasers Med. Sci.*, vol. 33, no. 6, pp. 1381–1386, Aug. 2018.
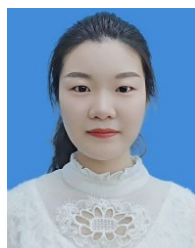
QIAN-LIN LIAN was born in Ürümqi, Xinjiang, China, in 1998. She received the bachelor's degree in information management and system from the School of Medical Engineering and Technology, Xinjiang Medical University, in 2020. She is currently pursuing the master's degree in epidemiology and health statistics with the School of Public Health, Xinjiang Medical University. Her present research interests include the intersection of medicine and engineering and laser-induced breakdown spectroscopy in biomedical field.

XIANG-YOU LI was born in Wuhan, China, in 1974. He received the Ph.D. degree in physics and electronics from the Huazhong University of Science and Technology (HUST), in 2005.

He was a fellow of the Japan Advanced Institute of Science and Technology (AIST), from 2009 to 2011. He is currently a researcher with the Wuhan National Laboratory of Opto-electronics, Huazhong University of Science and Technology, and a Chutian Scholar and a member of the Standing Committee of China Laser Induced Breakdown Spectroscopy. In recent years, he is mainly engaged in the software development of laser additive manufacturing technology (3D printing), the basic research of laser micro-nano manufacturing and processing technology, as well as the basic theory of laser-induced breakdown spectroscopy, instrument development, and engineering applications. He is a JSPS Fellow.

BING LU was born in Huanggang, Hubei, China, in 1991. He received the B.S. degree in mechanical engineering from the Wuchang Institute of Technology, Wuhan, China, in 2014, the M.S. degree in agricultural mechanical engineering from Tarim University, Alar, China, in 2017, and the Ph.D. degree in mechanical engineering from China Agricultural University, Beijing, China, in 2021.
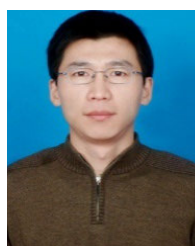
Since 2021, he has been a Postdoctoral Researcher with the Wuhan National Laboratory for Optoelectronics (WNLO), Huazhong University of Science and Technology. He is the author of more than 20 articles and more than 20 inventions. His research interests include agricultural machinery and equipment and atomic and molecular spectroscopy.

JIANG-TAO LI was born in Taiyuan, Shanxi, China, in September 1998. He received the B.S. degree in optoelectronic information science and engineering from the School of Testing and Electro-Optical Engineering, Nanchang Hangkong University (NCHU), China, in 2020, and the M.S. degree in optical engineering from the Huazhong University of Science and Technology (HUST), in 2022, with a focus on the technology of laser induced breakdown spectroscopy (LIBS), where he is currently pursuing the Ph.D. degree in electronic science and technology, with a focus on 3D printing.

CHEN-WEI ZHU was born in Dongying, Shandong, China, in 1996. She received the B.S. degree in forest products chemical processing from the School of Materials Science and Engineering, Northeast Forestry University (NEFU), China, in 2018, and the Ph.D. degree in optical engineering from the Huazhong University of Science and Technology (HUST), in 2023, with a focus on the technology of laser induced breakdown spectroscopy (LIBS).

JIAN-JUN CHEN was born in Shihezi, Xinjiang, China, in 1977. He received the B.Sc. degree in physics from Xinjiang Normal University, Ürümqi, Xinjiang, in 2001, and the M.Sc. and Ph.D. degrees in optics from Southwest University, Chongqing, China, in 2008 and 2017, respectively. He is currently a Professor with the School of Medical Engineering and Technology, Xinjiang Medical University. He is the author of more than 30 articles. His current research interests include nonlinear dynamics of semiconductor and application and laser-induced breakdown spectroscopy technology in biomedicine.

● ● ●